



Inverse spin Hall effect induced by spin pumping into semiconducting ZnO

Jung-Chuan Lee, Leng-Wei Huang, Dung-Shing Hung, Tung-Han Chiang, J. C. A. Huang, Jun-Zhi Liang, and Shang-Fan Lee

Citation: [Applied Physics Letters](#) **104**, 052401 (2014); doi: 10.1063/1.4863750

View online: <http://dx.doi.org/10.1063/1.4863750>

View Table of Contents: <http://scitation.aip.org/content/aip/journal/apl/104/5?ver=pdfcov>

Published by the [AIP Publishing](#)



FREE Multiphysics Simulation e-Magazine

DOWNLOAD TODAY >>

 COMSOL

Inverse spin Hall effect induced by spin pumping into semiconducting ZnO

Jung-Chuan Lee,¹ Leng-Wei Huang,² Dung-Shing Hung,^{1,3,a)} Tung-Han Chiang,⁴
 J. C. A. Huang,^{4,5,b)} Jun-Zhi Liang,^{5,6} and Shang-Fan Lee^{1,2,c)}

¹*Institute of Physics, Academia Sinica, Taipei 11529, Taiwan*

²*Graduate Institute of Applied Physics, National Chengchi University, Taipei 11605, Taiwan*

³*Department of Information and Telecommunications Engineering, Ming Chuan University, Taipei 111, Taiwan*

⁴*Department of Physics, National Cheng Kung University, Tainan 70101, Taiwan*

⁵*Advanced Optoelectronic Technology Center, National Cheng Kung University, Tainan 70101, Taiwan*

⁶*Department of Physics, Fu Jen Catholic University, Taipei 242, Taiwan*

(Received 2 December 2013; accepted 17 January 2014; published online 3 February 2014)

The inverse spin Hall effect (ISHE) of n-type semiconductor ZnO thin films with weak spin-orbit coupling has been observed by utilizing the spin pumping method. In the ferromagnetic resonance condition, the spin pumping driven by the dynamical exchange interaction of a permalloy film injects a pure spin current into the adjacent ZnO layer. This spin current gives rise to a DC voltage through the ISHE in the ZnO layer, and the DC voltage is proportional to the microwave excitation power. The effect is sizeable even when the spin backflow is considered. © 2014 AIP Publishing LLC. [<http://dx.doi.org/10.1063/1.4863750>]

Spintronics is an emerging technology, which has been extensively investigated in recent decades.¹ Spintronics deals with the intrinsic spin of individual electrons (or holes) and the collective behaviors of spins manifested as the magnetic moment in solid-state devices, which allows for the achievement of efficient magnetic memory chips and magnetic field sensing devices.¹ In such devices, generation, manipulation, and detection of the spin current are very important and necessary.^{2–6} Lately, the spin Hall effect (SHE) in nonmagnetic conductors has been recognized as playing a more active role in generating pure spin currents; and reversely, the spin currents can be detected by the inverse SHE (ISHE), fulfilling the functionality of spintronics devices.⁶ The spin Hall effect refers to the phenomenon that the spin-up and spin-down transport electrons accumulate transversely on opposite sides of a nonmagnetic conductor due to the spin-orbit coupling (SOC) that occurs without an external magnetic field.^{2,3} Consequently, the SHE can provide a simple physical mechanism to generate the transverse spin current by using the longitudinal charge current.^{2,3}

The SHE was first directly observed in gallium arsenide (GaAs) by utilizing the magneto-optical Kerr microscopy detection technique.⁴ However, the use of this technique was limited to direct band gap semiconductor.^{4,5} The probe of SHE in indirect band gap semiconductors with weak SOC (such as Si) was challenging.⁵ Hirsch proposed the concept of ISHE in 1999, in which the spin current is converted into a charge current through the SOC to be detected by electric measurements.³ The ISHE offers a simple way to explore the SHE in solids. Since then, many articles have been published on the topic of ISHE in the paramagnetic metals Pt, Au, Pd, Ta,^{6–19} and Si,⁵ GaAs,^{20,21} Ge²² semiconductors. The electric field E_{ISHE} generated by the ISHE can be expressed as^{5,12–14,18,20}

$$\mathbf{E}_{\text{ISHE}} = D_{\text{ISHE}} \mathbf{j}_s \times \boldsymbol{\sigma}, \quad (1)$$

where D_{ISHE} is a coefficient representing the ISHE efficiency in a material, \mathbf{j}_s and $\boldsymbol{\sigma}$ are the induced spin current and the spin-polarization unit vector, respectively.

There are several ways to generate a spin current such as the spin Seebeck effect^{23–25} and the spin pumping effect.^{5–20} In a ferromagnetic (FM)/nonmagnetic (NM) bilayer system, spin pumping drives a pure spin current from a ferromagnet into a normal metal via ferromagnetic resonance (FMR). Then the spin current is converted into a charge current through the ISHE, resulting in a detectable DC voltage.^{5,6}

Group II-VI semiconductor material Zinc Oxide (ZnO) has attracted a lot of attention lately for its prospects in optoelectronics applications owing to its direct wide band gap ($E_g \sim 3.3$ eV at 300 K) and large exciton binding energy (~ 60 meV).²⁶ ZnO has a small SOC ($\Delta_{\text{SO}} = 4\text{--}15$ meV)²⁷ implying a large spin coherence length. Being a conducting transparent semiconductor, ZnO is also a promising candidate for combining optoelectronics and spintronics applications.²⁸

In this work, the ZnO thin films were grown on *c*-plane sapphire (Al_2O_3) substrates by pulsed laser deposition (PLD). The deposition was carried out under an oxygen partial pressure of 1×10^{-5} Torr at 300 °C. A 248 nm KrF excimer laser with a frequency of 2 Hz and energy density of 120 mJ/cm² was used for deposition. The permalloy (Py, $\text{Ni}_{80}\text{Fe}_{20}$) layer was deposited onto the central part of the ZnO layer surface by ion-beam sputtering with a shadow mask. The base pressure was 1×10^{-6} Torr and the working pressure was 2×10^{-4} Torr of Argon (Ar). Then, the two tantalum (Ta) electrodes were deposited onto the edges of the ZnO layer by DC magnetron sputtering in 3×10^{-3} Torr of Ar. See Fig. 1(a) illustrates the schematics of the sample geometry. The thicknesses of the ZnO, Py, and Ta are 120 nm, 10 nm, and 10 nm, respectively. The measurements of the FMR responses and the ISHE of the samples were made by employing the flip-chip technique onto a coplanar waveguide, which is connected to an Agilent 8510C vector

^{a)}Electronic mail: dshung@mail.mcu.edu.tw

^{b)}Electronic mail: jc Huang@mail.ncku.edu.tw

^{c)}Electronic mail: leesf@phys.sinica.edu.tw

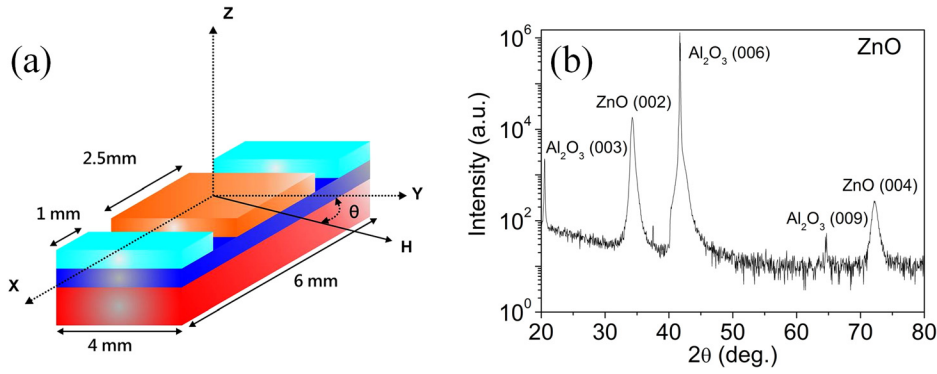


FIG. 1. (a) Schematic illustration of the ZnO/Py films. H represents an external magnetic field, angle θ is between the field and microwave propagation direction, Y axis, can be varied. (b) Shows the XRD spectra of ZnO films grown on Al_2O_3 substrates.

network analyzer. The coplanar waveguide is made out of 1.27 mm thick RT/Duroid 6010 substrate and has a central conductor 350 mm long, 0.6 mm wide, and 0.35 mm gaps to the ground on both sides. The microwave field distribution and the comparison to other FMR techniques can be found in the literature.²⁹

The ZnO has n-type conductivity caused by the presence of oxygen vacancies or zinc interstitials.²⁶ The resistivity, the carrier concentration, and the mobility are 0.014 Ω cm, $6.09 \times 10^{18} \text{ cm}^{-3}$, and 72.9 $\text{cm}^2/\text{V s}$, respectively. The structural analysis of ZnO was obtained by θ -2 θ X-ray diffraction (XRD) measurements, which shows the wurtzite structure with c -axis preferred orientations as shown in Fig. 1(b).

The FMR spectra of the ZnO/Py film in different in-plane external magnetic field H values from 0.5 GHz to 3.5 GHz are displayed in Fig. 2(a). The FMR absorption

frequency vs. H for the ZnO/Py film is shown in the inset of Fig. 2(a). The experimental data can be fitted by the Kittel formula^{9,11,14}

$$(f/\gamma)^2 = H_{\text{FMR}}(H_{\text{FMR}} + 4\pi M_s), \quad (2)$$

where $\gamma = 2.8 \text{ GHz/kOe}$ is the gyromagnetic ratio, H_{FMR} is the resonance magnetic field, and M_s is the saturation magnetization. Fig. 2(b) exhibits the H dependence of DC voltage V measured for the ZnO/Py under 50 mW microwave excitation at the in-plane field angle $\theta = 0$ as defined in Fig. 1(a). The DC voltages all have maximum values in the FMR condition. The results are consistent with Fig. 2(a), verifying that the voltage is indeed due to the ISHE.⁵⁻²² In the FMR condition, the precessing magnetization of Py is driven by dynamic exchange interaction and injects a pure spin current into the ZnO layer, and the electric field E_{ISHE} is generated by the ISHE from the spin current density, j_s , with the spin-polarization vector σ as described in Eq. (1). As a result, the DC voltage $V_{\text{ISHE}} = w_F E_{\text{ISHE}}$ can be measured, where w_F is the width of the ferromagnetic layer.¹⁴ In addition to the ISHE, the anisotropic magnetoresistance (AMR) effect in Py should be considered, too. The DC voltage is a superposition of the contributions from spin pumping (V_{ISHE}) and AMR (V_{AMR}), which can be distinguished by their symmetries. It can be expressed as a function of the in-plane field angle θ ^{11,30,31}

$$V_{\text{dc}}(H, \theta) = V_{\text{AMR}}[L(H)\cos\phi + L'(H)\sin\phi]\sin(2\theta)\sin\theta + V_{\text{ISHE}}L(H)\cos\theta, \quad (3)$$

where $L(H) = \frac{\Delta H^2}{(H-H_{\text{FMR}})^2 + \Delta H^2}$ is the symmetric Lorentzian function, $L'(H) = \frac{\Delta H(H-H_{\text{FMR}})}{(H-H_{\text{FMR}})^2 + \Delta H^2}$ is an antisymmetric function, ΔH is the linewidth of the resonance, and ϕ is the phase difference between the coupled current and the magnetization precession. The V_{ISHE} only has a symmetric component, but the V_{AMR} has both symmetric and antisymmetric components. For $\theta = 0^\circ$ and 180° , the V_{AMR} does not contribute to the DC voltage. Fig. 3(a) shows magnetic field dependence of the DC voltage of ZnO/Py under 50 mW microwave excitation at 1.8 GHz for $\theta = 0^\circ$ and 180° . A clear voltage signal appears in the FMR condition, and the voltage signal reverses when the H direction is reversed, which is consistent with Eqs. (1) and (3), supporting that the voltage is due to ISHE induced by the spin pumping.^{8,10,11,17,18,20,22} The solid lines show the fitting results using a Lorentz function,

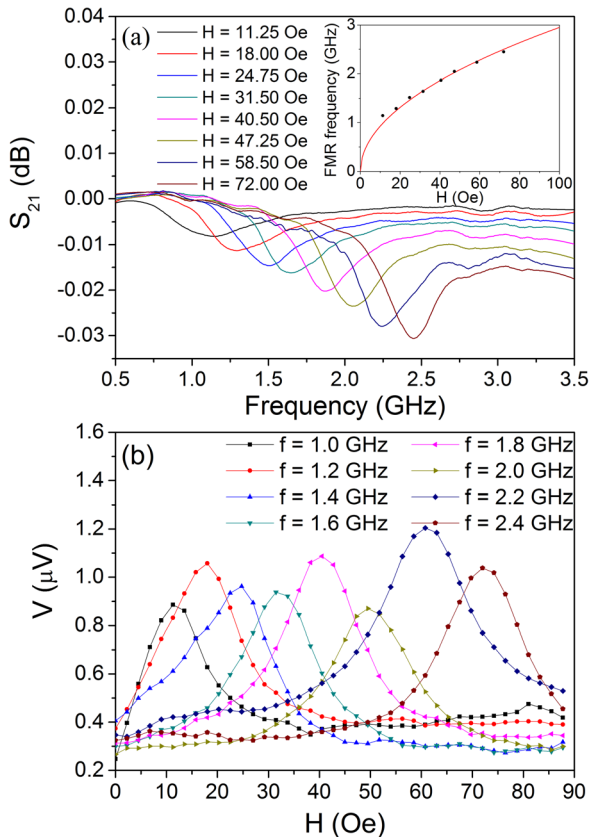


FIG. 2. (a) The FMR spectra of ZnO/Py, and the inset is magnetic field H dependence of FMR frequency for ZnO/Py. (b) Magnetic field H dependence of DC voltage V measured for the ZnO/Py under 50 mW microwave excitation.

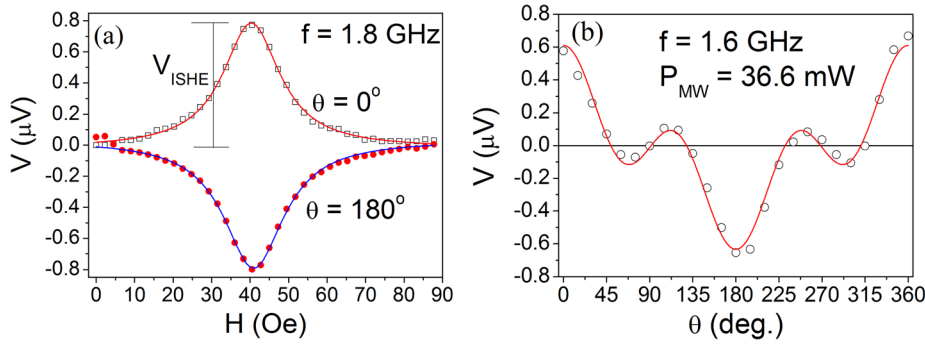


FIG. 3. (a) Magnetic field H dependence of the electromotive force V of $\text{Ni}_{80}\text{Fe}_{20}/\text{ZnO}$ thin film under 50 mW microwave excitation, where θ are 0° and 180° . The solid lines show the fitting results using the Lorentz function. V_{ISHE} is estimated as the peak height of the resonance shape in the V spectra. (b) Shows the in-plane angle θ dependence of the electromotive force V for ZnO/Py . The hollow symbols are the experimental data, and the solid line is a fitting line.

implying the voltage only arises from the ISHE. Our data support that the voltage signal is attributed to the spin pumping effect.^{10,11,30,31} Fig. 3(b) exhibits the in-plane angle θ dependence of the DC voltage V for ZnO/Py . The applied microwave power is 36.6 mW, and the frequency is 1.6 GHz. Since we are measuring DC voltage, the microwave magnetic field contributes to our angular dependence measurements through the noise but not directly. The hollow symbols are the experimental data, and the solid line is the least square fitting line by Eq. (3). The best fit gives $V_{\text{AMR}} = -0.52$ V and $V_{\text{ISHE}} = 0.62$ V.

The V_{ISHE} is estimated as the peak height of the resonance shape in the V spectra in Fig. 2(b), and the microwave power P_{MW} dependence of V_{ISHE} for the ZnO/Py bilayer at $\theta = 0^\circ$ and 180° is shown in the inset of Fig. 4. The V_{ISHE} is proportional to the microwave power P_{MW} , satisfying the phenomenological model of the DC spin pumping^{14,18}

$$V_{\text{ISHE}} = \frac{W_F \theta_{SH} \lambda_N \tanh\left(\frac{d_N}{2\lambda_N}\right)}{d_N \sigma_N + d_F \sigma_F} \left(\frac{2e}{\hbar}\right) j_s^0, \quad (4)$$

where $j_s^0 = \frac{g_r^{\uparrow\downarrow} \gamma^2 \hbar^2 h_{rf}^2 [4\pi M_s \gamma + \sqrt{(4\pi M_s)^2 \gamma^2 + 4\omega^2}]}{8\pi \alpha^2 [(4\pi M_s)^2 \gamma^2 + 4\omega^2]}$, and $g_r^{\uparrow\downarrow}$ is the real part of spin mixing conductance, h_{rf} is the amplitude of the microwave magnetic field, α is the Gilbert damping constant, ω is the microwave angular frequency, σ_N and σ_F are the conductivities, and d_N and d_F are the thicknesses of the ZnO and Py layers, respectively.

The spin mixing conductance $g_r^{\uparrow\downarrow}$ is the essential parameter to the spin pumping experiment. It refers to the

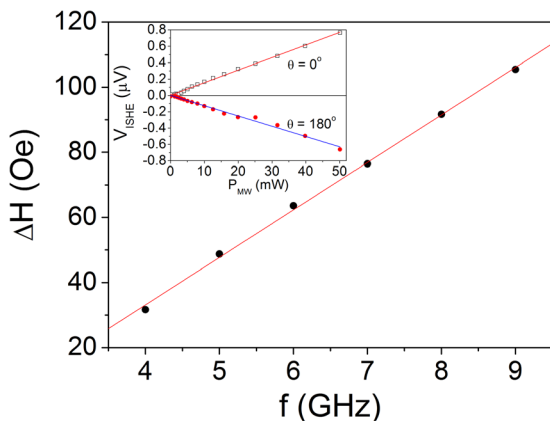


FIG. 4. FMR linewidth as a function of microwave frequency for ZnO/Py . The inset shows microwave power P_{MW} dependence of V_{ISHE} for the ZnO/Py bilayer at $\theta = 0^\circ$ and 180° .

efficiency of generating a spin current across the interface and is related to the Gilbert damping coefficient α as³²

$$\sigma = \frac{g\mu_B}{4\pi M_s d_F} g_r^{\uparrow\downarrow}. \quad (5)$$

The damping coefficient can be evaluated from the linewidth (ΔH) of the FMR measurements from the linear dependence of ΔH on the microwave frequency³²

$$\Delta H_{\text{FMR}} = \Delta H_0 + \frac{2\alpha}{\gamma} f. \quad (6)$$

Our experimental results on ZnO/Py films are shown in Fig. 4. From the linear fitting, the damping coefficient $\alpha = 0.02$ and $g_r^{\uparrow\downarrow} = 5.4 \times 10^{14} \text{ cm}^{-2}$ can be obtained by Eq. (5). This α value is reasonable for spin pumping experiments utilizing Py . The $g_r^{\uparrow\downarrow}$ value is comparable to the reported value for Si , but larger than that for GaAs .^{5,20}

Although we have measured the ISHE in ZnO/Py bilayers, the origin of V_{ISHE} still should be explored carefully. The ISHE originates from SOC, and the magnitude of intrinsic SOC is proportional to the atomic number raised to the power of four (Z^4). Considering the weak spin-orbit interaction in ZnO semiconductors, we further discuss this clear ISHE signal below. Recently, Jiao and Bauer analyzed the ISHE in FM/NM bilayers and emphasized the spin backflow phenomenon theoretically. The spin current resulting from the spin accumulation near the interface not only flows into the NM but also into the FM as well.³³ The spin backflow converts into a charge current due to the SOC and generates an electric field in FM, too. Therefore, the electric field of the FM/NM bilayers can be expressed as³³

$$E_y = \frac{2e/\hbar}{\sigma_N d_N + \sigma_F d_F} \left[\vec{j}_{1s}^z(0) \theta_{SH}^N \lambda_{sd}^N \tanh \frac{d_N}{2\lambda_{sd}^N} + \vec{j}_{2s}^z(0) \theta_{SH}^F \lambda_{sd}^F \tanh \frac{d_F}{2\lambda_{sd}^F} \right], \quad (7)$$

where $\vec{j}_{1s}^z(0)$ and $\vec{j}_{2s}^z(0)$ are the spin currents at the interface of the NM and FM sides, θ_{SH}^N and θ_{SH}^F are the spin Hall angles, and λ_{sd}^N and λ_{sd}^F are the spin diffusion lengths of NM and FM, respectively. In Eq. (7), the first term comes from the ISHE in NM, and the second term is due to the anomalous Hall effect (AHE) in FM. Tsukahara *et al.*³⁴ and Miao *et al.*²⁵ showed that the ISHE of Py was non-negligible

experimentally and estimated the spin Hall angle θ_{SH} of Py to be 0.005–0.01. In Ref. 34, Tsukahara considered that since AMR, AHE, and ISHE are from the same origin, SOC, then the ISHE in Py should not be neglected. They grew Py on two kinds of insulated substrates, SiO₂ and YIG (Yttrium Iron Garnet), and discovered the V_{ISHE} of Py/YIG was far weaker than Py/SiO₂. Their results demonstrated that the local spin damping at the Py/SiO₂ interface can induce a spin density gradient, which allowed diffusive flow of spin current in the Py layer near the interface, and resulted in the ISHE. Because the magnetization damping of YIG is weak, the V_{ISHE} observed in Py/YIG is very small. Nevertheless, for our samples, ZnO is a semiconductor and not an insulator. The spin current should partially flow into ZnO and partially backflow into Py, converting both into V_{ISHE} because of SOC. Therefore, the measured V_{ISHE} is contributed from both ZnO and Py simultaneously.

According to Eq. (7), the V_{ISHE} 's of ZnO and Py are proportional to $\vec{j}_{1s}^N(0)\theta_{SH}^N\lambda_{sd}^N\tanh\frac{d_N}{2\lambda_{sd}^N}$ and $\vec{j}_{2s}^F(0)\theta_{SH}^F\lambda_{sd}^F\tanh\frac{d_F}{2\lambda_{sd}^F}$. Although we do not have the spin Hall angle and spin diffusion length of ZnO, we can refer to the data of Si due to the fact that ZnO and Si are both semiconductors with very small spin-orbit interaction. The θ_{SH} and λ of Si are 0.0001 and 200–300 nm, respectively.^{5,35} The θ_{SH} and λ of Py are 0.005 and 3.3–5.5 nm, respectively.^{36,37} We assume that $\vec{j}_{1s}^N(0)\tanh\frac{d_N}{2\lambda_{sd}^N}$ is equal to $\vec{j}_{2s}^F(0)\tanh\frac{d_F}{2\lambda_{sd}^F}$, and then the V_{ISHE} ratio of ZnO to Py is $\theta_{SH}^N\lambda_{sd}^N:\theta_{SH}^F\lambda_{sd}^F$, which is about 5:4. Therefore, the V_{ISHE} of ZnO contribution in the total measured DC voltage is estimated to be over 50%.

In this work, the ISHE in ZnO semiconductors has been observed by spin pumping. The DC voltage signals changed with the excitation microwave frequencies, power levels, and the in-plane angle θ of the external magnetic field H . All the results indicate that the voltage signals are due to the ISHE induced by spin pumping and confirm that the ISHE can be observed even in weak spin-orbit coupling materials like ZnO.

The financial support of the Academia Sinica and the National Science Council of Taiwan, Republic of China are gratefully acknowledged.

¹S. A. Wolf, D. D. Awschalom, R. A. Buhrman, J. M. Daughton, S. von Molnár, M. L. Roukes, A. Y. Chtchelkanova, and D. M. Treger, *Science* **294**, 1488 (2001).

²M. I. Dyakonov and V. I. Perel, *Phys. Lett. A* **35**, 459 (1971).

³J. E. Hirsch, *Phys. Rev. Lett.* **83**, 1834 (1999).

⁴Y. K. Kato, R. O. Myers, A. C. Gossard, and D. D. Awschalom, *Science* **306**, 1910 (2004).

⁵K. Ando and E. Saitoh, *Nat. Commun.* **3**, 629 (2012).

- ⁶E. Saitoh, M. Ueda, H. Miyajima, and G. Tatara, *Appl. Phys. Lett.* **88**, 182509 (2006).
- ⁷K. Ando, S. Takahashi, K. Harii, K. Sasage, J. Ieda, S. Maekawa, and E. Saitoh, *Phys. Rev. Lett.* **101**, 036601 (2008).
- ⁸O. Mosendz, V. Vlaminck, J. E. Pearson, F. Y. Fradin, G. E. W. Bauer, S. D. Bader, and A. Hoffmann, *Phys. Rev. B* **82**, 214403 (2010).
- ⁹O. Mosendz, J. E. Pearson, F. Y. Fradin, G. E. W. Bauer, S. D. Bader, and A. Hoffmann, *Phys. Rev. Lett.* **104**, 046601 (2010).
- ¹⁰R. Takahashi, R. Iguchi, K. Ando, H. Nakayama, T. Yoshino, and E. Saitoh, *J. Appl. Phys.* **111**, 07C307 (2012).
- ¹¹A. Azevedo, L. H. Vilela-Leão, R. L. Rodríguez-Suárez, A. F. Lacerda Santos, and S. M. Rezende, *Phys. Rev. B* **83**, 144402 (2011).
- ¹²Y. Kajiwara, K. Harii, S. Takahashi, J. Ohe, K. Uchida, M. Mizuguchi, H. Umezawa, H. Kawai, K. Ando, K. Takanashi, S. Masekawa, and E. Saitoh, *Nature* **464**, 262 (2010).
- ¹³K. Ando, S. Takahashi, J. Ieda, Y. Kajiwara, H. Nakayama, T. Yoshino, K. Harii, Y. Fujikawa, M. Matsuo, S. Maekawa, and E. Saitoh, *J. Appl. Phys.* **109**, 103913 (2011).
- ¹⁴H. Nakayama, K. Ando, K. Harii, T. Yoshino, R. Takahashi, Y. Kajiwara, K. Uchida, and Y. Fujikawa, *Phys. Rev. B* **85**, 144408 (2012).
- ¹⁵M. Harder, Z. X. Cao, Y. S. Gui, X. L. Fan, and C.-M. Hu, *Phys. Rev. B* **84**, 054423 (2011).
- ¹⁶K. Ando, T. Yoshino, and E. Saitoh, *Appl. Phys. Lett.* **94**, 152509 (2009).
- ¹⁷E. Shikoh, K. Ando, K. Kubo, E. Saitoh, T. Shinjo, and M. Shiraishi, *Phys. Rev. Lett.* **110**, 127201 (2013).
- ¹⁸Y. Kitamura, E. Shikoh, Y. Ando, T. Shinjo, and M. Shiraishi, *Sci. Rep.* **3**, 1739 (2013).
- ¹⁹L. Liu, C. F. Pai, Y. Li, H. W. Tseng, D. C. Ralph, and R. A. Buhrman, *Science* **336**, 555 (2012).
- ²⁰K. Ando, S. Takahashi, J. Ieda, H. Kurebayashi, T. Trypiniotis, C. H. W. Barnes, S. Maekawa, and E. Saitoh, *Nature Mater.* **10**, 655 (2011).
- ²¹K. Olejník, J. Wunderlich, A. C. Irvine, R. P. Campion, V. P. Amin, J. Sinova, and T. Jungwirth, *Phys. Rev. Lett.* **109**, 076601 (2012).
- ²²M. Koike, E. Shikoh, Y. Ando, T. Shinjo, S. Yamada, K. Hamaya, and M. Shiraishi, *Appl. Phys. Express* **6**, 023001 (2013).
- ²³T. Kikkawa, K. Uchida, Y. Shiomi, Z. Qiu, D. Hou, D. Tian, H. Nakayama, X.-F. Jin, and E. Saitoh, *Phys. Rev. Lett.* **110**, 067207 (2013).
- ²⁴D. Qu, S. Y. Huang, J. Hu, R. Wu, and C. L. Chien, *Phys. Rev. Lett.* **110**, 067206 (2013).
- ²⁵B. F. Miao, S. Y. Huang, D. Qu, and C. L. Chien, *Phys. Rev. Lett.* **111**, 066602 (2013).
- ²⁶Ü. Özgür, Ya. I. Alivov, C. Liu, A. Teke, M. A. Reshchikov, S. Doğan, V. Avrutin, S.-J. Cho, and H. Morkoç, *J. Appl. Phys.* **98**, 041301 (2005).
- ²⁷W. M. Chen, I. A. Buyanova, A. Murayama, T. Furuta, Y. Oka, D. P. Norton, S. J. Pearton, A. Osinsky, and J. W. Dong, *Appl. Phys. Lett.* **92**, 092103 (2008).
- ²⁸M. Althammer, E.-M. Karrer-Muller, S. T. B. Goennenwein, M. Peel, and R. Gross, *Appl. Phys. Lett.* **101**, 082404 (2012).
- ²⁹I. Neudecker, G. Woltersdorf, B. Heinrich, T. Okuno, G. Gubbiotti, and C. H. Back, *J. Magn. Magn. Mater.* **307**, 148 (2006).
- ³⁰L. Bai, Z. Feng, P. Hyde, H. F. Ding, and C.-M. Hu, *Appl. Phys. Lett.* **102**, 242402 (2013).
- ³¹T. D. Skinner, H. Kurebayashi, D. Fang, D. Heiss, A. C. Irvine, A. T. Hindmarch, M. Wang, A. W. Rushforth, and A. J. Ferguson, *Appl. Phys. Lett.* **102**, 072401 (2013).
- ³²E. Th. Papaioannou, P. Fuhrmann, M. B. Jungfleisch, T. Brächer, P. Pirro, V. Lauer, J. Lösch, and B. Hillebrands, *Appl. Phys. Lett.* **103**, 162401 (2013).
- ³³H. Jiao and G. E. W. Bauer, *Phys. Rev. Lett.* **110**, 217602 (2013).
- ³⁴A. Tsukahara, Y. Ando, and Y. Kitamura, e-print [arXiv:1301.3580](https://arxiv.org/abs/1301.3580).
- ³⁵R. Jansen, *Nature Mater.* **11**, 400 (2012).
- ³⁶S. Zhang and S. S.-L. Zhang, *Phys. Rev. Lett.* **102**, 086601 (2009).
- ³⁷S. Dubois, L. Piraux, J. M. George, K. Ounadjela, J. L. Duval, and A. Fert, *Phys. Rev. B* **60**, 477 (1999).